What Global Modelers Want to Know About Terrestrial Ion Outflow

B. L. Giles and T. E. Moore
[NASA Goddard Space Flight Center, Code 692, Greenbelt, MD 20771, USA,
barbara.giles@gsfc.nasa.gov]

Abstract: Application of published terrestrial outflow studies to the broader problem of globally modeling the flow's impact on magnetosphere dynamics is complicated by several factors. It is important to apply corrections to derived fluxes for convection drifts or for the effects of spacecraft potential. Also, because acceleration processes take place along a distributed altitude range, it is not clear which portions of the reported flows types will reach escape velocity and therefore reach the inner boundary of global magnetospheric models. We seek to address these issues by providing a description of the terrestrial outflows capable of populating and influencing the magnetosphere outside of 3 RE altitude and by demonstrating, via particle simulations, the conditions under which this outflow can influence plasma sheet dynamics. The description, both statistical and functional, is of the terrestrial ion outflow for energies below 300 eV associated with auroral and polar latitude processes. The simulations demonstrate the conditions under which dayside and nightside outflows access the near-Earth transitional region and the more distant neutral point region, as a function of interplanetary parameters observed to drive the flows.

Nominal Strength of the Flow

Escaping Fluxes at Source

	Solar Maximum			Solar Minimum			
	H+	He+	O+	H+	He+	O+	Comments:
Quiet Conditions							
Polar wind	5.00E+07	6.00E+06	–	3.00E+08	3.85E+06	–	Chappell et al., 1987, Chandler et al., 1991
Cusp/Cleft	1.20E+07	1.20E+07	3.20E+08	1.20E+07	1.20E+07	8.00E+06	Pollock et al., 1990, present work
Auroral zone	4.00E+06	4.00E+06	4.00E+07	4.00E+06	4.00E+06	1.00E+06	present work
Polar cap							
Active Conditions							
Polar Wind	1.50E+08	2.00E+07	–	2.00E+08	1.82E+06	–	Chappell et al., 1987, Chandler et al., 1991
Cusp/Cleft	6.00E+08	3.00E+08	4.00E+09	6.00E+08	3.00E+08	4.00E+08	Pollock et al., 1990, present work
Auroral zone	2.00E+08	1.00E+08	5.00E+08	2.00E+08	1.00E+08	5.00E+07	present work
Polar Cap				2.00E+07		1.00E+06	Su et al, 1998

Accumulated Escaping Fluxes

	Solar Maximum			Solar Minimum			
	H+	He+	O+	H+	He+	O+	
Quiet Conditions							
Polar wind	8.50E+24	1.02E+24	–	5.10E+25	6.55E+23	–	
Cusp/Cleft	9.60E+23	9.60E+23	2.56E+25	9.60E+23	9.60E+23	6.40E+23	
Auroral zone	3.20E+23	3.20E+23	3.20E+24	3.20E+23	3.20E+23	8.00E+22	
Polar cap	4.00E+24		8.00E+24	6.50E+24		2.00E+24	Yau and Andre,1999
Total	1.38E+25	2.30E+24	3.68E+25	5.88E+25	1.93E+24	2.72E+24	
Total ions		5.29E+25			6.34E+25		
Active Conditions							
Polar Wind	2.55E+25	3.40E+24	–	3.40E+25	3.09E+23	–	
Cusp/Cleft	2.40E+25	1.20E+25	1.60E+26	2.40E+25	1.20E+25	1.60E+25	
Auroral zone	8.00E+24	4.00E+24	2.00E+25	8.00E+24	4.00E+24	2.00E+24	
Polar Cap	1.50E+25		4.50E+25	2.05E+25		1.70E+25	Yau and Andre,1999
Total	7.25E+25	1.94E+25	2.25E+26	8.65E+25	1.63E+25	3.50E+25	
Total Ions		3.17E+26			1.38E+26		

The Minimum Level of Escaping Outflow

The figure to the right is an overview plot of the maximum upward ion flux for Polar/TIDE H^+, He^+ and O^+ upwelling events in 1996 and includes events at all local times and geocentric altitudes from 1.81 to 2.27 R_E. At solar minimum, the measured fluxes for H^+ range over several orders of magnitude from $4.x10^6$ to $2\ x10^8$ $cm^{-2}s^{-1}$ with a mean value of $6.5\ x10^7$ $cm^{-2}s^{-1}$. The upward velocities tend toward 40.7 ± 20.6 km/s. For He+, the measured fluxes range from $2.x10^5$ to $9\ x10^7$ $cm^{-2}s^{-1}$ with a mean value of $2\ x10^7$ $cm^{-2}s^{-1}$. O^+ upward fluxes range from $\sim 7 \times 10^5$ to 5×10^7 $cm^{-2}s^{-1}$ with a mean value of 1.1×10^7 $cm^{-2}s^{-1}$. Upward velocities tend toward 2.4 ± 1.2 km/s.

The second figure in this box shows an ion upwelling observed as Polar/TIDE crossed the nightside auroral zone during the May 10-12, 1999 "day the solar wind disappeared". The solar wind density and velocity averaged 0.67 cm^{-3} and 384 km/s, respectively, for the half hour preceding this observation. The figure shows that fluxes of $2. \times 10^7$ to $2. \times 10^8$ $cm^{-2}s^{-1}$ (total ion measurement) should not be considered unusual even for the quietest magnetosphere.

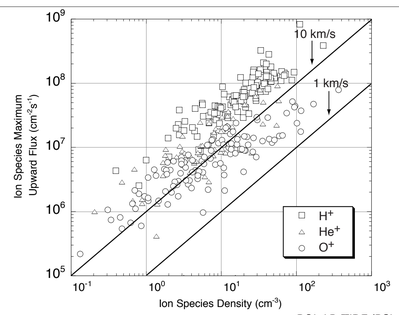

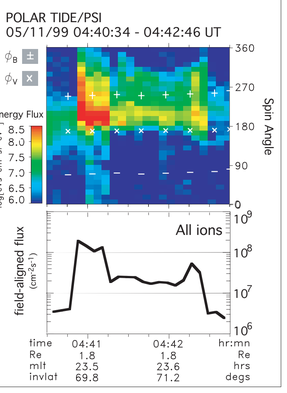

The Maximum Level of Escaping Outflow

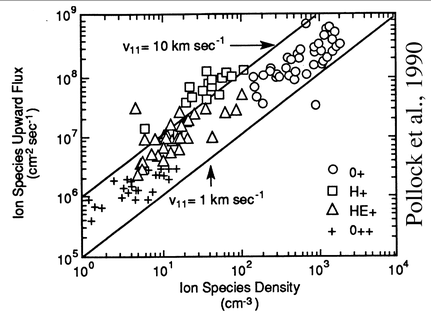

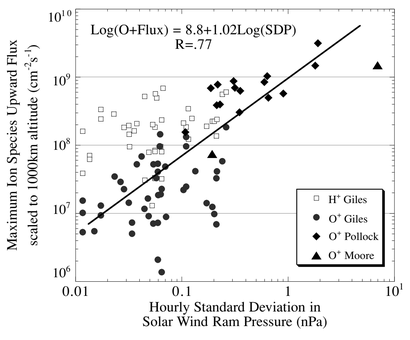

The figure to the left is an overview plot similar to the one above except for DE-1/RIMS H^+, He^+, O^+ and O^{++} upwelling events under solar maximum conditions. Note the similar flux levels between solar maximum and minimum conditions for H^+ and He^+ but not for O^+. At solar min, O^+ upward fluxes average 1.1×10^7 $cm^{-2}s^{-1}$ with an upward velocity averaging 2.4 ± 1.2 km/s. At solar max, the fluxes range from $5x10^7$ to $1.x10^9$ $cm^{-2}s^{-1}$ at 2-3 km/s, a two order of magnitude difference. The format of the plot shows that the flux difference at solar maxmum is due to enhanced heavy ion densities rather than an increase in bulk flow velocity.

The second figure compares trends in the Polar/TIDE and DE-1/RIMS data sets with the variability in the solar wind momentum flux. There is a consistent increase in escaping ion flux across the full range of pressure variation. Rather than the second order effects demonstrated by various IMF correlations, the variability in solar wind dynamic pressure well accounts for the range of fluxes in the figures above.

The GSFC/GM Empirical Model: Schematic

Sources of Terrestrial Plasma
- Cleft Ion Fountain
- Auroral Ion Fountain
- Polar Wind
- Polar Cap

The quantities, density (n_i) and field-aligned flux (F_{para}) are given by the expression:

$$A(r, f, q) = A_{cf} + A_{af} + A_{pw} + A_{pc}$$

A_{cf}, A_{af}, A_{pw}, and A_{pc} represent the contribution from the plasmasphere, the cleft ion fountain, and auroral ion fountain, polar wind and polar cap, respectively.

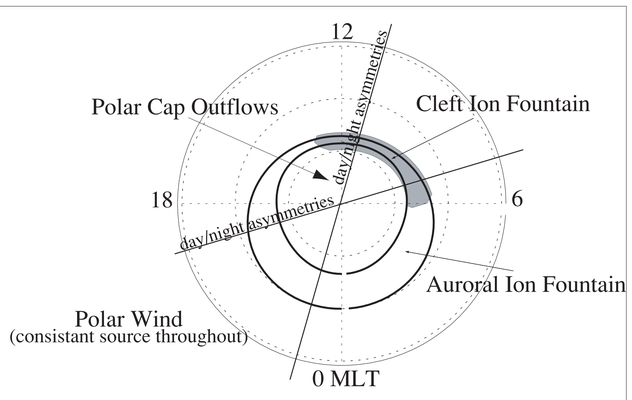

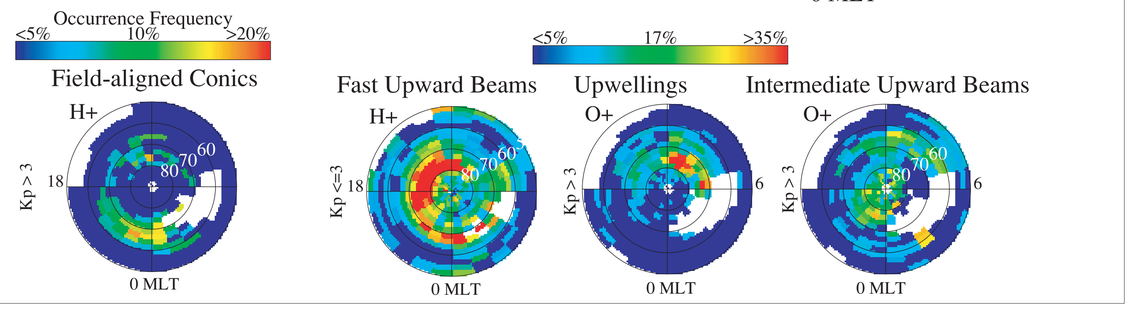

The GSFC/GM Empirical Model: Auroral Outflows

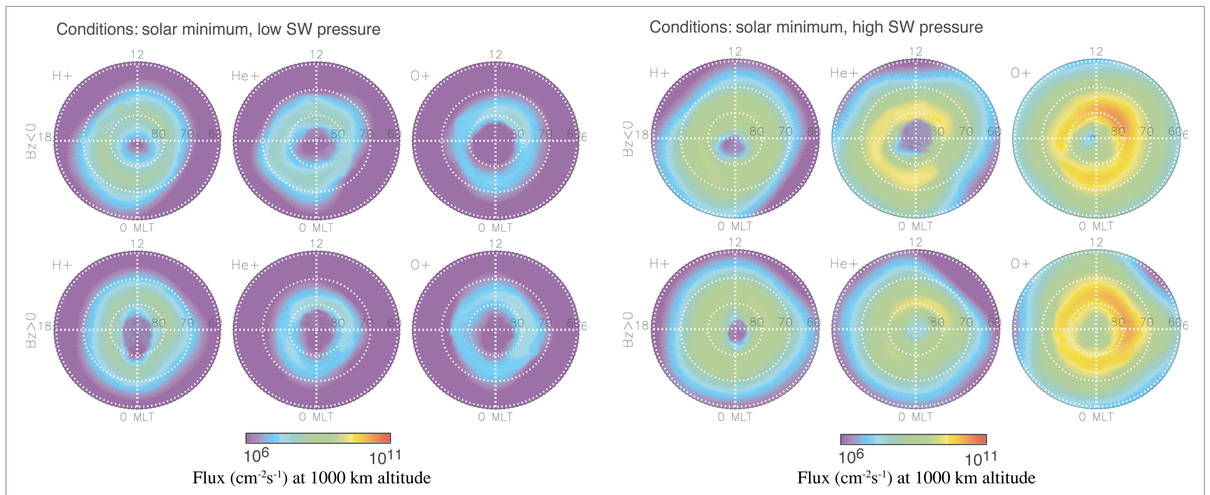

Formulation of the Model: Auroral Outflows

Density coefficients / **Field aligned flux coefficients**

		p_0	C_0	C_1	S_0	S_1	p_0	C_0	C_1	S_0	S_1
H^+											
all	f_{max}	14.433	-3.514	5.451	-2.266	-5.231	1.52E+08	6.40E+06	1.20E+07	3.65E+07	-7.69E+07
	$ilat_o$	78.634	-1.488	0.281	-2.823	0.098	77.782	-1.646	-0.575	-3.893	0.184
	S_1	0.209	0.127	0.042	0.017	0.143	0.209	0.042	0.022	0.026	-0.031
	S_2	-0.260	-0.076	0.027	0.173	-0.038	-0.251	-0.076	0.086	0.149	-0.016
$B_z \le 0$	f_{max}	13.781	-5.192	2.071	3.338	-4.144	1.83E+08	9.28E+06	1.96E+06	5.40E+07	-8.46E+07
	$ilat_o$	75.794	-0.544	-0.183	-0.119	2.913	75.985	-0.468	-0.204	0.056	2.566
	S_1	0.243	-0.050	0.227	0.040	-0.125	0.184	-0.094	0.126	-0.053	-0.110
	S_2	-0.219	-0.052	0.027	0.161	-0.021	-0.227	-0.037	0.045	0.144	0.014
$B_z > 0$	f_{max}	14.746	-6.164	9.109	-2.046	-10.719	1.44E+08	-1.26E+07	4.41E+07	2.34E+07	-8.83E+07
	$ilat_o$	78.092	-1.551	-0.265	-3.257	-0.675	78.153	-2.049	-0.292	-3.000	-0.187
	S_1	0.167	0.000	0.009	-0.081	0.051	0.181	0.102	0.054	0.024	-0.103
	S_2	-0.273	-0.110	0.118	0.079	0.095	-0.264	-0.064	0.032	0.199	-0.024
He^+		p_0	C_0	C_1	S_0	S_1	p_0	C_0	C_1	S_0	S_1
all	f_{max}	7.001	-2.381	3.036	-0.303	-1.424	3.74E+07	-1.54E+07	2.78E+06	1.11E+07	-1.60E+07
	$ilat_o$	78.824	-0.726	-0.551	-3.241	0.224	76.391	-1.342	2.583	-1.151	1.173
	S_1	0.254	0.099	0.024	0.128	-0.172	0.123	-0.044	-0.065	0.057	-0.029
	S_2	-0.192	0.102	0.012	0.132	-0.013	-0.199	0.137	0.048	0.079	0.010
$B_z \le 0$	f_{max}	7.430	-2.585	1.127	1.040	0.103	6.09E+07	-2.72E+07	-1.87E+07	1.10E+07	-1.33E+07
	$ilat_o$	76.448	-1.622	2.455	-0.550	1.958	76.199	-1.596	3.399	-0.904	0.958
	S_1	0.265	0.028	-0.095	-0.047	-0.107	0.218	0.047	-0.137	0.094	0.004
	S_2	-0.140	-0.022	-0.032	0.033	0.031	-0.164	0.071	-0.062	-0.012	0.083
$B_z > 0$	f_{max}	7.147	-3.319	4.429	-1.790	-2.716	3.12E+07	-1.80E+07	2.46E+06	3.57E+06	-1.04E+07
	$ilat_o$	79.162	-1.347	-0.863	-2.676	0.263	76.792	-1.905	2.023	-0.785	0.897
	S_1	0.131	0.062	0.092	0.085	-0.008	0.242	0.051	-0.031	0.153	-0.073
	S_2	-0.216	0.060	0.033	0.033	-0.035	-0.238	0.124	0.030	0.041	-0.050
O^+		p_0	C_0	C_1	S_0	S_1	p_0	C_0	C_1	S_0	S_1
all	f_{max}	20.021	-10.622	15.996	-3.020	-3.212	1.92E+07	-1.12E+07	1.20E+07	6.71E+04	-6.17E+06
	$ilat_o$	79.791	-2.617	-0.036	-2.649	0.684	77.419	-2.609	-1.546	-3.002	-0.308
	S_1	0.186	0.035	0.006	0.107	0.059	0.204	0.163	0.056	0.094	-0.056
	S_2	-0.276	0.041	0.057	0.125	0.046	-0.183	-0.079	0.011	-0.004	0.009
$B_z \le 0$	f_{max}	19.950	-17.771	4.646	-0.192	2.889	2.65E+07	-1.79E+07	2.19E+07	-4.13E+06	-1.17E+07
	$ilat_o$	77.001	-2.891	0.009	0.230	1.559	74.946	-2.885	0.029	0.652	-0.086
	S_1	0.149	0.110	0.109	0.017	0.063	0.264	0.068	0.125	0.049	-0.085
	S_2	-0.228	0.117	-0.009	-0.135	-0.023	-0.117	-0.017	-0.018	-0.090	0.013
$B_z > 0$	f_{max}	17.247	-6.608	15.113	-1.283	-5.153	1.69E+07	-1.05E+07	1.05E+07	1.95E+06	-9.36E+06
	$ilat_o$	78.625	0.335	-1.019	-3.538	-1.521	78.035	-1.621	-0.600	-3.477	-0.674
	S_1	0.177	0.000	0.043	-0.014	0.011	0.212	0.030	-0.032	0.090	0.075
	S_2	-0.325	-0.037	0.067	0.069	0.112	-0.249	-0.116	-0.009	0.039	0.102

Following the example of *Hardy et al.* [1987], the patterns of auroral outflowing ion flux and density are represented using fits to Epstein transition functions.

$$f(ilat,mlt,index) = f_{max} + S_1(ilat\text{-}ilat_o) + (S_2\text{-}S_1) \cdot \ln\{[1\text{-}S_1/(S_2 e^{-(ilat\text{-}ilato)})]/[1\text{-}(S_1/S_2)]\}$$

Here, f_{max} is the maximum value of the quantity to be fit; ilat is the invariant latitude in degrees, $ilat_o$ is the invariant latitude at the maximum value; S_1 is the slope of the curve for invariant latitudes less than $ilat_o$; S_2 is the curve slope for invariant latitudes greater than $ilat_o$.

A functional form for the local time dependence of the Epstein function parameters is constructed using a Fourier series,

$$p(mlt,index) = p_o(index) + \Sigma\{C_n \cos[n(mlt/12)] + S_n \sin[n(mlt/12)]\}$$

Here, p(mlt,index) refers to the parameter to be represented, p(mlt,index) = fmax, $ilat_o$; S_1; and S_2. The Fourier coefficients and the initial parameter value vary with the activity index or IMF range chosen.

In this manner, each parameter of the Epstein transition function is represented using a total of n+1 coefficients, and a complete map of auroral outflow or density is represented by 4(n+1) coefficients. **The table to the left** contains the coefficients derived for changing IMF Bz direction.

SM22A-08

Ionosphere Plasma Access to the Plasma Sheet: Nominal Conditions

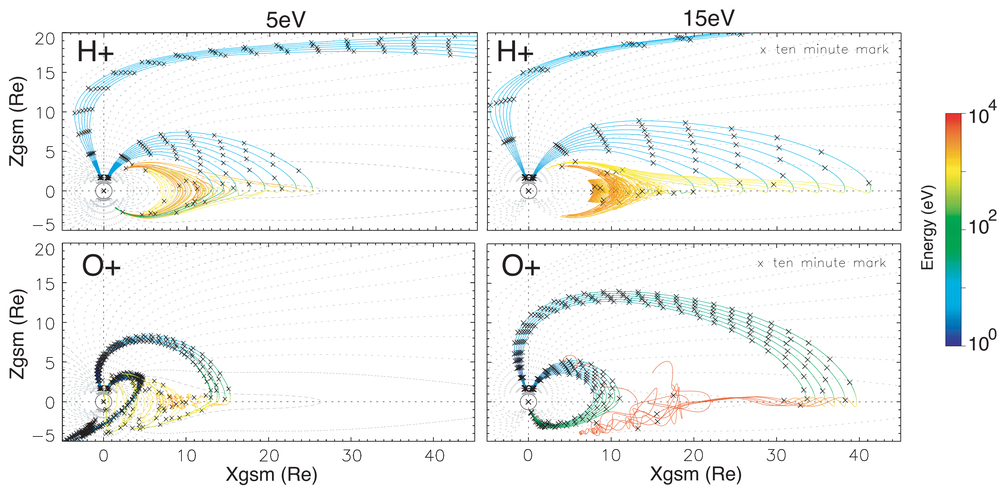

The Figure above shows magnetosphere regions accessible to ionosphere outflows by calculating **E** x **B** convection paths, via complete equations of motion within the magnetic field model of *Tsyganenko* [1987] for Kp=0 and a modified *Volland* [1978] electric field with cross tail potential drop of 25 kV. H^+ and O^+ ions are launched using characteristic upwelling source altitude and energy parameters.

The H^+ particles launched at noon convect antisunward and remain at large distances from the equator eventually escaping toward the magnetotail. The O^+ particles launched at noon and the H^+ nightside trajectories adiabatically intercept the center plane at distances that depend on the initial latitude, approaching the neutral sheet in a nearly field-aligned manner and with increasing energy from the sharply increasing curvature drift. Upon encountering the neutral sheet, centrifugal trapping and the subsequent nonadiabatic motion within the neutral sheet (*Delcourt et al.* [1994]) produce further energization and earthward traveling stochastic trajectories typical of the energetic plasma sheet. The trajectories have been arbitrarily discontinued once convecting inside of 10 R_E or exiting simulation boundaries. Nightside O^+ feeds directly into the near Earth closed magnetic field-line region becoming bidirectional corotating distributions. These particle simulations demonstrate the active role of low-energy ionospheric ions throughout the most dynamic regions of the magnetosphere even for very quiet, solar minimum conditions.

Ionosphere Plasma Access to the Plasma Sheet: Intermediate Conditions

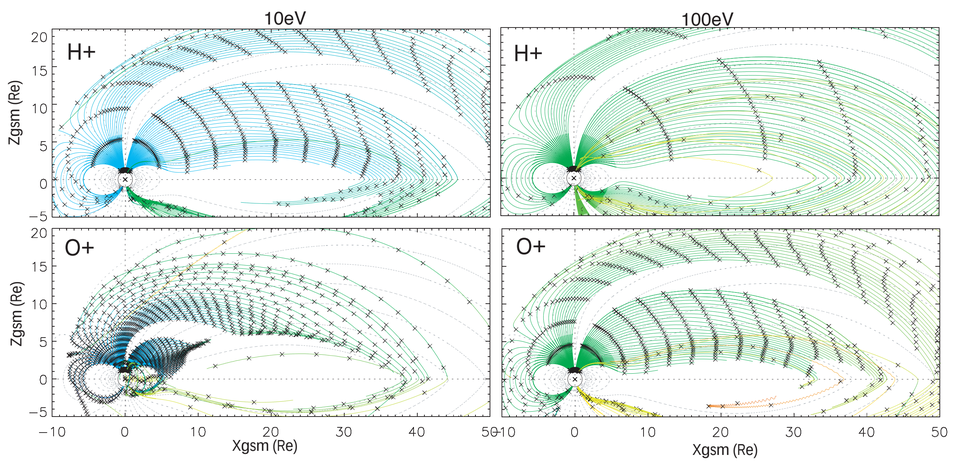

Same as the figure above but for Kp=3 and a cross tail potential drop of 35 kV and the addition of an enhanced near-Earth current system to describe the observed development of the tail magnetic field during the growth phase.

Ionosphere Plasma Access to the Plasma Sheet: Active Conditions

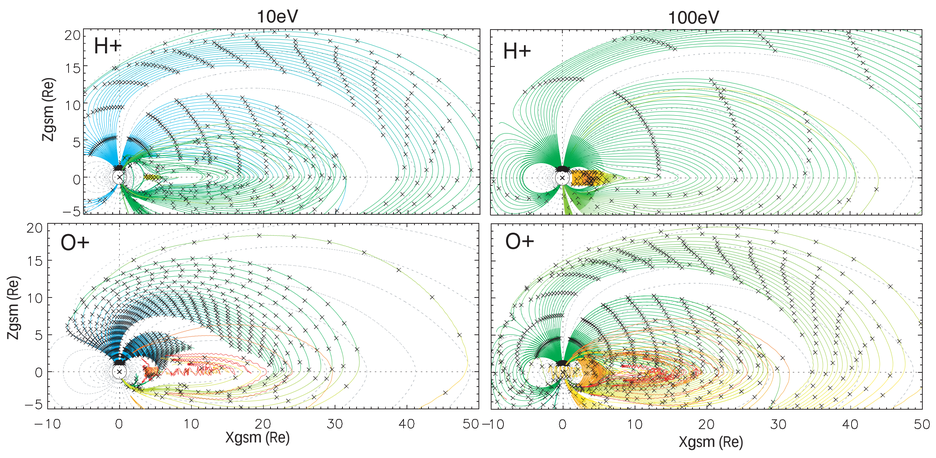

Same as the figure above but for Kp=3 and a cross tail potential drop of 35 kV and the addition of an enhanced near-Earth current system to describe the observed development of the tail magnetic field during the growth phase.

Thermal Plasma in the Plasma Sheet: October 9, 2001

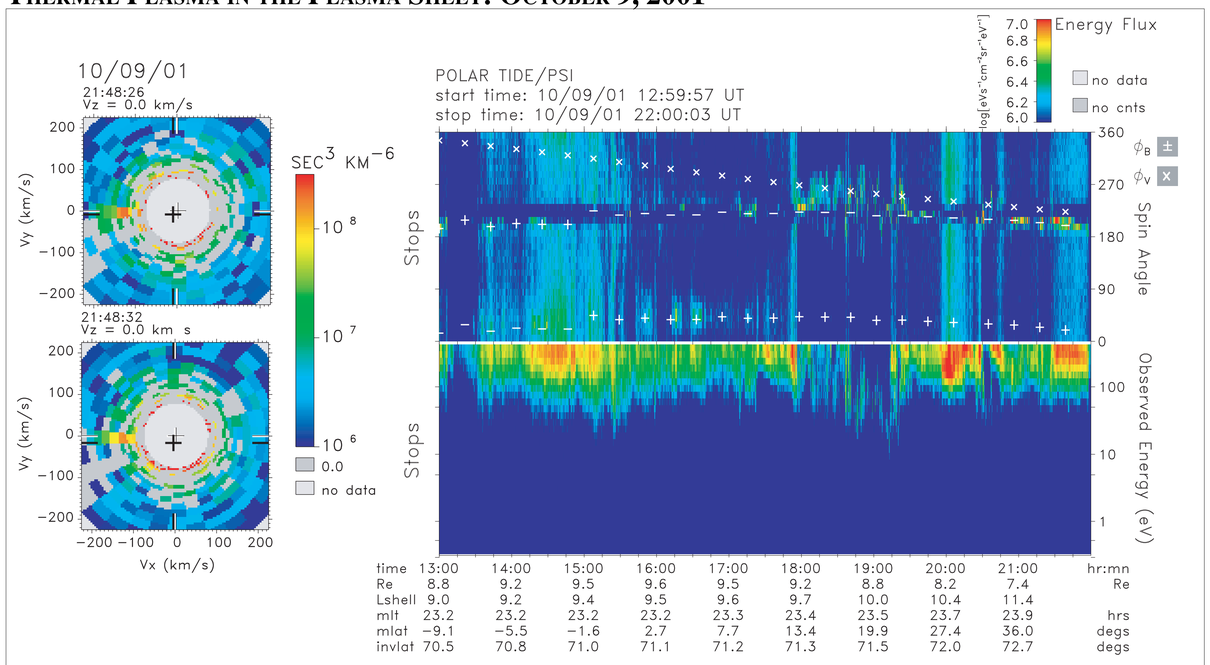

Observations of low energy ionospheric plasma entering the plasma sheet boundary layer. Note the magnetic field reversal at ~1500UT where the field changes from sunward to antisunward in a distance of ~500 km. Field-aligned beams are clearly streaming tailward from ~2100-2200UT. DST ranged from -38 to -74, IMF was generally northward but with several southward turnings.

Thermal Plasma in the Plasma Sheet: October 22, 2001

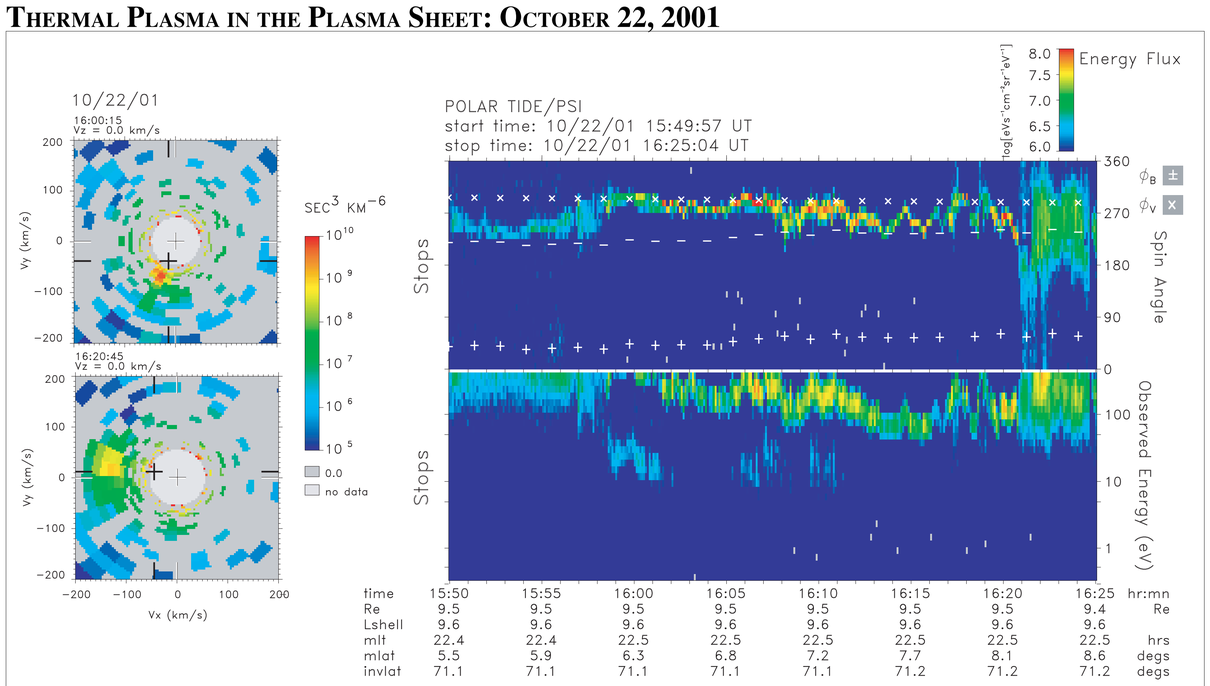

Similar to the case above although for more dynamic conditions (DST<-150, southward Bz). Notice that hints of lighter ion species are present from ~1600-1610UT. The high activity level produced enhanced ionospheric plasma energies allowing detection of this normally hidden plasma population over the substantial spacecraft potentials typical at these altitudes.

Reminder: Consequences of Spacecraft Charging on Thermal Plasma Measurements

Two examples are shown of the Polar spacecraft potential as measured by the Polar/EFI instrument at altitudes between 7 and 9 Re. Also shown are Polar/TIDE thermal plasma distributions for two time periods during the observation run. The top panel represents nominal conditions with no spacecraft potential control. The bottom panel represents conditions when the spacecraft potential is clamped to ~2.4V.

Thermal field-aligned beams of the type shown in the bottom panel are not resolvable without active spacecraft potential control.

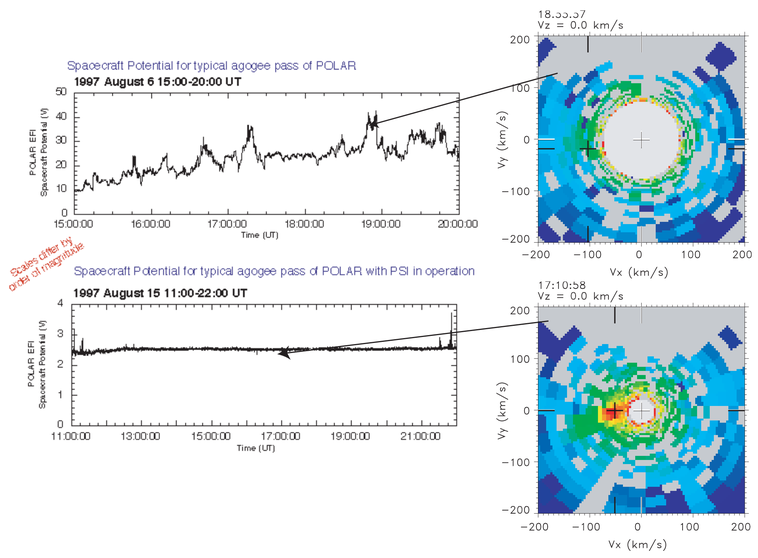

References:

Andre M., and A. Yau, Theories and observations of ion energization and outflow in high latitude magnetosphere, Space Sci. Rev., 80, 27-48, 1997.Delcourt, D. C., and G. Belmont, Ion dynamics at the earthward termination of the magntotail current sheet., J. Geophys. Res., 103, 4605-4613, 1998.

Chandler, M. O., J. H. Waite, Jr., and T. E. Moore, Observations of polar wind outflows, J. Geophys. Res., 96, 1421-1428, 1991.

Chappell. C. R., t. E. Moore and J. H. Waite, Jr., The ionosphere as a fully adequate source of plasma for the Earth's magnetosphere, J. Geophys. Res., 5896-5910, 1987.

Delcourt, D. C., T. E. Moore and C. R. Chappell, Contribution of low-energy ionosphere protons to the plasma sheet, *J. Geophys. Res., 99*, 5681-5689, 1994.

Delcourt, D. C., and G. Belmont, Ion dynamics at the earthward termination of the magnetotail current sheet, J. Geophys. Res., 4605-4613, 1998.

Hardy, D. A., M. S. Gussenhoven, R. Raistrick, and W. J. McNeil, Statistical and functional representations of the pattern of auroral energy flux, number flux and conductivity, J. Geophys. Res., 92, 12,275-12,294. 1987.

Pollock, C. J., M. O. Chandler, T. E. Moore, J. H. Waite, Jr., C. R. Chappell, and D. A. Gurnett, A survey of upwelling ion event characteristics, *J. Geophys. Res., 95,* 18969-18,980, 1990.

Pulkkinen, T. I., D. N. Baker, D. H. Fairfield, R. J. Pellinen, J. S. Murphree, R. D. Elphinstone, R. L. McPherron, J. F. Fennell, R. E. Lopez, and T. Nagai, Modeling the growth phase of a substorm using the Tsyganenko model and multi-spacecraft observations: CDAW-9, Geophys. Res., Lett., 18, 1963-1966, 1991.

Su, Yi-Jiun, J. L. Horwitz, T. E. Moore, B. L. Giles, M. O. Chandler, P. D. Craven, M. Hirahara, and C. J. Pollock, J. Geophys. Res., 103, 29,305-29,337, 1998.